J. Fluid Mech. (1996), *vol.* 314, *pp.* 315–330

An inverse energy cascade in two-dimensional low Reynolds number bubbly flows

By ASGHAR ESMAEELI AND GRÉTAR TRYGGVASON

Department of Mechanical Engineering and Applied Mechanics, The University of Michigan, Ann Arbor, MI 48109, USA

(Received 26 April 1995 and in revised form 15 January 1996)

Two direct numerical simulations of several buoyant bubbles in a two-dimensional periodic domain are presented. The average rise Reynolds number of the bubbles is close to 2, and surface tension is high, resulting in small bubble deformation. The void fraction is relatively high, and the bubbles interact strongly. Simulations of the motion of both 144 and 324 bubbles show the formation of flow structures much larger than the bubble size, and a continuous increase in the energy of the low-wavenumber velocity modes. Plots of the energy spectrum show a range of wavenumbers with an approximately $-5/3$ slope. This suggests that a part of the work done by the buoyant bubbles is not dissipated, but instead increases the energy of flow structures much larger than the bubbles. This phenomenon, which is also seen in numerical simulation of forced two-dimensional turbulence, prevents the appearance of a statistically steady-state motion that is independent of the size of the computational domain.

1. Introduction

While direct numerical simulations of complex unsteady single-phase flows have become a standard research tool in fluid mechanics, simulations of multiphase flows are much less common. Generally, such simulations are limited to the isothermal motion of two-fluid systems with a relatively simple geometry, such as a single drop or a bubble. In most engineering systems, however, it is the collective behaviour of a very large number of bubbles, drops, or particles that is of interest. For engineering predictions, averaged equations for mean quantities and low-order statistics are employed (see Drew 1983 and Drew & Lahey 1993 for example). However, the averaging results in unknown terms that must be modelled. Such models are analogous to closure models for the Reynolds stresses in turbulent single-phase flows, but involve the forces due to the interactions between the phases in addition to momentum transfer by velocity fluctuations. As for single phase flows, the fundamental small-scale interactions can not be addressed unless the range of scales investigated is large enough. Therefore, simulations of a large number of bubbles, drops, or particles are required.

In this paper we present the results of direct simulations of the unsteady motion of 144 and 324 two-dimensional bubbles in a fully periodic domain. The work is motivated by several simulations of systems containing a relatively small number of bubbles described in Esmaeeli & Tryggvason (1996*a*). There, each simulation reached an approximately steady state relatively quickly, but the results did not appear to

converge as the size of the system (number of bubbles) was increased. To address this issue, we undertook the simulations described here. The main observation is that unlike systems with a small number of bubbles, the large systems do not seem to settle down to a steady state during the time we simulated. Instead, larger and larger flow structures continue to emerge. Although somewhat surprising at first, this behaviour has been seen before in numerical simulations of two-dimensional turbulence. After presenting our results and discussing their relation to two-dimensional turbulence, we conclude with a few remarks about the relation of these results to other systems as well as the implication for modelling of multiphase flows.

Other simulations of systems with several bubbles, drops, or particles at finite Reynolds numbers are limited to work done by Feng, Hu, & Joseph (1994) who simulated the two-dimensional, unsteady motion of up to four rigid particles, Unverdi & Tryggvason (1992*a*,*b*) who computed the interactions of two two- and three-dimensional bubbles, and Esmaeeli & Tryggvason (1996*a*,*b*) (see also Esmaeeli 1995) who simulated the unsteady motion of several two- and three-dimensional bubbles. Esmaeeli & Tryggvason used sixteen bubbles in most of their two-dimensional computations and up to eight for their three-dimensional simulations. In the zero Reynolds number limit, where all inertia effects are neglected (Stokes flow), a few researchers have simulated reasonably complex flows. Brady and coworkers have followed the motion of several particles in both two and three dimensions using a multipole expansion technique (see Brady & Bossis 1988; Brady 1993), Zhou & Pozrikidis (1993, 1994) simulated the evolution of up to twelve two-dimensional, fully deformable drops in a shear flow using a boundary integral technique, and Manga & Stone (1993) computed the interaction of two three-dimensional drops in the same way. For very high Reynolds numbers, the motion of several bubbles has been modelled by simulating the evolution of spheres in a potential flow. See, for example, Sangani & Prosperetti (1993), Sangani & Didwania (1993), and Smereka (1993).

For a more thorough discussion of the use of numerical simulations for investigations of multiphase flows, including a more extensive literature survey, see Esmaeeli & Tryggvason (1996*a*).

2. Formulation and numerical method

The computational domain is a doubly periodic square box, such that bubbles that leave through one boundary will reappear through the opposite boundary. The Navier–Stokes equations are valid for both fluids, and a single set of equations can be written for the whole domain as long as the jump in viscosity and density is correctly accounted for and surface tension is included:

$$\frac{\partial \rho \boldsymbol{u}}{\partial t} + \nabla \cdot \rho \boldsymbol{u}\,\boldsymbol{u} = -\nabla p + (\rho_0 - \rho)\boldsymbol{g} + \nabla \cdot \mu(\nabla \boldsymbol{u} + \nabla \boldsymbol{u}^T) + \sigma \int \frac{\partial \boldsymbol{t}}{\partial s}\delta(\boldsymbol{x} - \boldsymbol{x}_f')\mathrm{d}A'. \quad (2.1)$$

Here, $\boldsymbol{u}$ is the velocity, p is the pressure, ρ and μ are the discontinuous density and viscosity fields, respectively, and σ is the constant surface tension coefficient. Interfacial forces are added at the interface between the bubbles and the ambient liquid and δ is a two-dimensional delta function. The integral is over the bubble surface. This results in a force that is smooth along the surface of the bubble. $\boldsymbol{t}$ is a tangent vector to the bubble surface and s is an arclength coordinate. Carrying out the differentiation leads to the usual expression for the surface tension, $\sigma \boldsymbol{n} \kappa$, where $\boldsymbol{n}$ is a normal vector and κ is the curvature. The form written down here is the one we use in our code. For periodic domains, we need to impose additional constrains

to prevent uniform acceleration of the whole flow field in the direction of gravity. Here, we add a body force, $\rho_0 \boldsymbol{g}$, where ρ_0 is the average density, to the equations for this purpose. This ensures that the net flux of momentum through the computational domain is zero. If the bubbles were completely massless, this would be equivalent to imposing no net throughflow of liquid. However, since the density of the bubbles is finite here, their upward motion is accompanied by a slight net downward motion of the liquid. This motion is very small.

The momentum equations are supplemented by the incompressibility condition:

$$\nabla \cdot \boldsymbol{u} = 0 \tag{2.2}$$

which, when combined with the momentum equations leads to a non-separable elliptic equation for the pressure. The density and viscosity of each fluid is constant.

The rise of a single buoyant bubble is governed by four non-dimensional numbers. Two of those are the ratios of the dispersed phase (gas) density and viscosity to those of the continuous phase (liquid): $\gamma = \rho_b/\rho_o$ and $\lambda = \mu_b/\mu_o$. Here, the subscript o denotes the ambient liquid and b stands for the gas in the bubble. Once these ratios are sufficiently small, their influence on the motion is small. The remaining two numbers can be selected in a number of ways. If we pick the density of the outer fluid, ρ_o, the effective diameter of the bubble, d_e, and the gravity acceleration, g, to make the other variables dimensionless we obtain

$$N = \frac{\rho_o{}^2 d_e{}^3 g}{\mu_o{}^2}; \qquad Eo = \frac{\rho_o g d_e{}^2}{\sigma}.$$

The first number is sometimes called the Gallileo or the Archimedes number (see Clift, Grace & Weber 1978) and is a Reynolds number squared based on the velocity scale $(gd_e)^{1/2}$. The second one is usually called the Eötvös number. In the chemical engineering literature, N is usually replaced by the Morton number, $M = g\mu_o^4/\rho_o\sigma^3 = Eo^3/N^2$, which is constant for a given fluid if the gravity acceleration is constant. For bubbly clouds where many bubbles rise together, the void fraction α, defined as the volume of the dispersed phase divided by the total volume, must also be specified and for more complex flow fields, such as a shear flow, additional parameters are needed. When presenting our results we non-dimensionalize time by $(d_e/g)^{1/2}$ and length by the bubble diameter.

The numerical technique used for the simulations presented in this paper is the Front Tracking/Finite Difference method of Unverdi & Tryggvason (1992*a*,*b*). The procedure has been described in detail there. The Navier–Stokes equations are solved on a fixed, uniform, staggered grid and discretized using a conservative, second-order centred difference scheme for the spatial variables and an explicit second-order time integration. The novelty of the scheme is the way the boundary, or the front, between the bubbles and the ambient liquid is tracked. The front is represented by separate computational points that are moved by interpolating their velocities from the grid. These points are connected by line elements to form a front that is used to keep the density and viscosity stratification sharp and to calculate surface tension. At each time step information must be passed between the front and the stationary grid. The density jump is distributed to the grid points next to the front to generate a smooth density field that changes from one density to the other over two to three grid spaces. While this replaces the sharp interface by a slightly smoother grid interface, all numerical diffusion of the density jump is eliminated since the grid field is reconstructed at each time step. Once the density has been found, the viscosity is set as a function of the density. The pressure equation, which is non-separable due

to the difference in density between the bubbles and the ambient fluid, is solved by a multigrid package ("MUDPACK", see Adams 1989). The method and the code have been tested in various ways, such as by extensive grid refinement studies, comparison with other investigations and analytical solutions. In Jan & Tryggvason (1996) we compared our results using an axisymmetric implementation of the method used here with one of the cases computed by Ryskin & Leal (1984) ($Re = 20$ and $We = 12$) and found our rise velocity to be within 2% of theirs for a bubble resolved by about 25 grid points per radius (and a large enough computational domain so that wall effects could be ignored). In the same paper we also compared our results with analytical results for the rise of a bubble in a pipe in the limit of zero Reynolds number and found less than 2% error for similar resolution. Resolution tests using the two-dimensional code used here are presented in Esmaeeli & Tryggvason (1996*a*), where we report grid refinement studies for both a single bubble as well as for a system of 16 bubbles. The governing parameters were the same as used here. Generally, the resolution requirement decreases with Reynolds number and the resolution used here, about 13 grid points per bubble diameter, resulted in essentially the same evolution as a run with about 20 points per bubble diameter, although the rise velocity on the coarser grid was slightly lower (3% for the single bubble and 5% for the 16 bubble system).

3. Results

Here we present the results of two simulations of the evolution of 144 and 324 two-dimensional bubbles in a doubly periodic domain. The governing parameters are selected in such a way that the rise Reynolds number is low and the bubbles remain nearly cylindrical. The void fraction is relatively high so the bubbles interact strongly. The computations are done in a domain that is 12 by 12 units for the 144 bubble run and 18 by 18 units for the 324 bubble run. In both cases the effective diameter of each bubble is 0.4 units. (Although the volume of each bubble remains constant, they generally deform slightly and are exactly circular only at $t = 0$). Gravity is set to 1, and the fluid density and viscosity are 25 and 1.12468, respectively. The surface tension coefficient is 4.0. The density and viscosity of the gas are one twentieth of the corresponding liquid properties. In terms of the non-dimensional numbers introduced in the preceding section, we have

$$Eo = 1.0;\ N = 10^{3/2}\ (M = 10^{-3});\ \gamma = 0.05;\ \lambda = 0.05;\ \alpha = 0.1256.$$

For these parameters a single two-dimensional bubble in a doubly periodic domain will have a rise Reynolds number of 1.6 which is comparable with that given in figure 2.5 in Clift *et al.* (1978) for a three-dimensional bubble in an unbounded fluid. These values of the non-dimensional parameters could, for example, be realized using air bubbles of diameter 1.9 mm in standard engine oil (taking $\sigma = 0.03$ N m^{-1}, $\rho = 880$ kg m^{-3}, and $\mu = 0.21$ N s m^{-2}), with the exception that the density and viscosity ratios would be lower. However, extensive tests with lower ratios of the material properties (down to 1/300) have shown that the effect of the bubble density and viscosity are already very small for the values used here, see Esmaeeli (1995). The 144 bubble computation is done on a grid with 386^2 mesh points and was run up to non-dimensional time 175.6, while the 324 bubble computation was done on a 578^2 grid and run up to non-dimensional time 147.9. The size of the time step was constant and the total number of time steps was about 41000 and 35500 for the 144 and the 324 bubble runs, respectively. The computations took 33 s per time step for the 144 bubble run and 82 s per time step for the 324 bubble run on an IBM-SP1

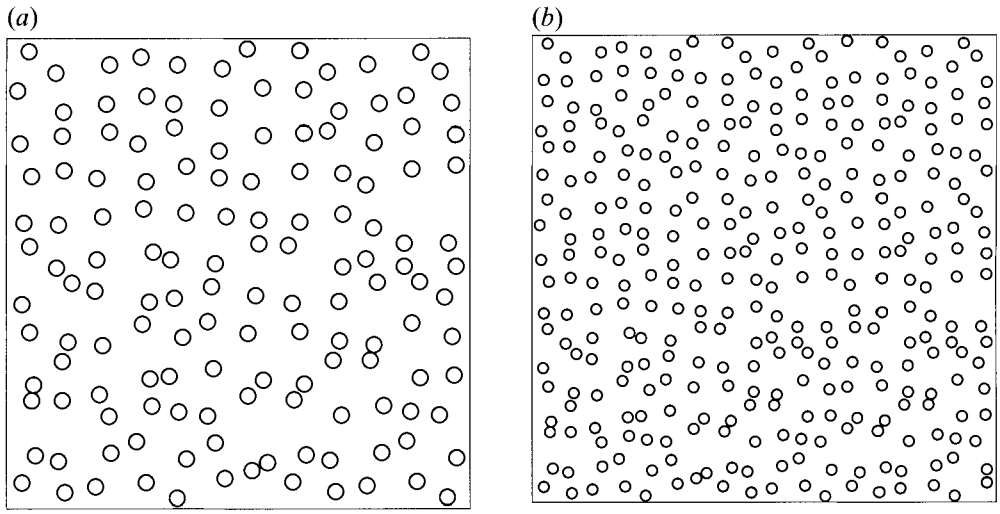

FIGURE 1. The initial conditions for the 144 bubble simulation (*a*) and the 324 bubble simulation (*b*). The resolution used is 386^2 and 578^2 grid points, respectively.

workstation. The initial positions of the bubbles were set by starting with regular arrays of bubbles, 12 by 12 and 18 by 18, and 'manually' perturbing their positions in a quasi-random way. Figure 1 shows the initial conditions for both runs.

Figure 2 shows two frames from the 144 bubble run. Both the bubble surfaces and the velocity field, plotted at every 6th grid point, are shown. The times are selected near the beginning of the run ($t = 15.8$, in *a*) and at the end of the run ($t = 175.6$, in *b*). The velocity vectors are scaled by the same constant in both frames, and it is immediately obvious that the velocities are generally larger at the later time. While the flow field at the early time is relatively irregular, in several places there are 'streams' of fast moving upward flow driven by several bubbles lining up in tandem. At the later time there is a well-defined up-flow region near the right boundary of the domain and a distinct, although not quite as uniform, down-flow region in the middle of the domain. We also note that while the bubbles are relatively evenly distributed at time zero, the result at later time shows both regions with relatively high concentration of bubbles and regions which are nearly free of bubbles. Similar evolution is also seen in figure 3, where we plot the bubble configuration at two times for the 324 bubble simulation. Figure 3(*a*) shows the results at time 15.8, and 3(*b*) at time 147.9. Instead of the velocities, here we plot twenty equispaced streamfunction contours. The streamfunction plots show clearly the emergence of flow structures that are many times larger than the bubbles, and that the size of these structures is much larger at the later time. As we may expect, the up-flow regions generally contain a high concentration of bubbles, but the down-flow is, for the most part, void of bubbles.

The details of the flow field around each bubble are not very clear in figures 2 and 3, so in figure 4 we plot the velocity field and the bubbles for the small rectangular region outlined near the middle of figure 3(*b*). Here, the velocity is plotted at every grid point, and it is clear that even the smallest length scales of the flow field are well resolved.

In figure 5 we plot the average rise Reynolds number of the bubbles versus time, for both runs. Both simulations show a slow increase in the average rise Reynolds number, and although the detailed evolution of the bubbles is very different, the averages are in relatively good agreement. We note that giving the rise velocity in terms of a Reynolds

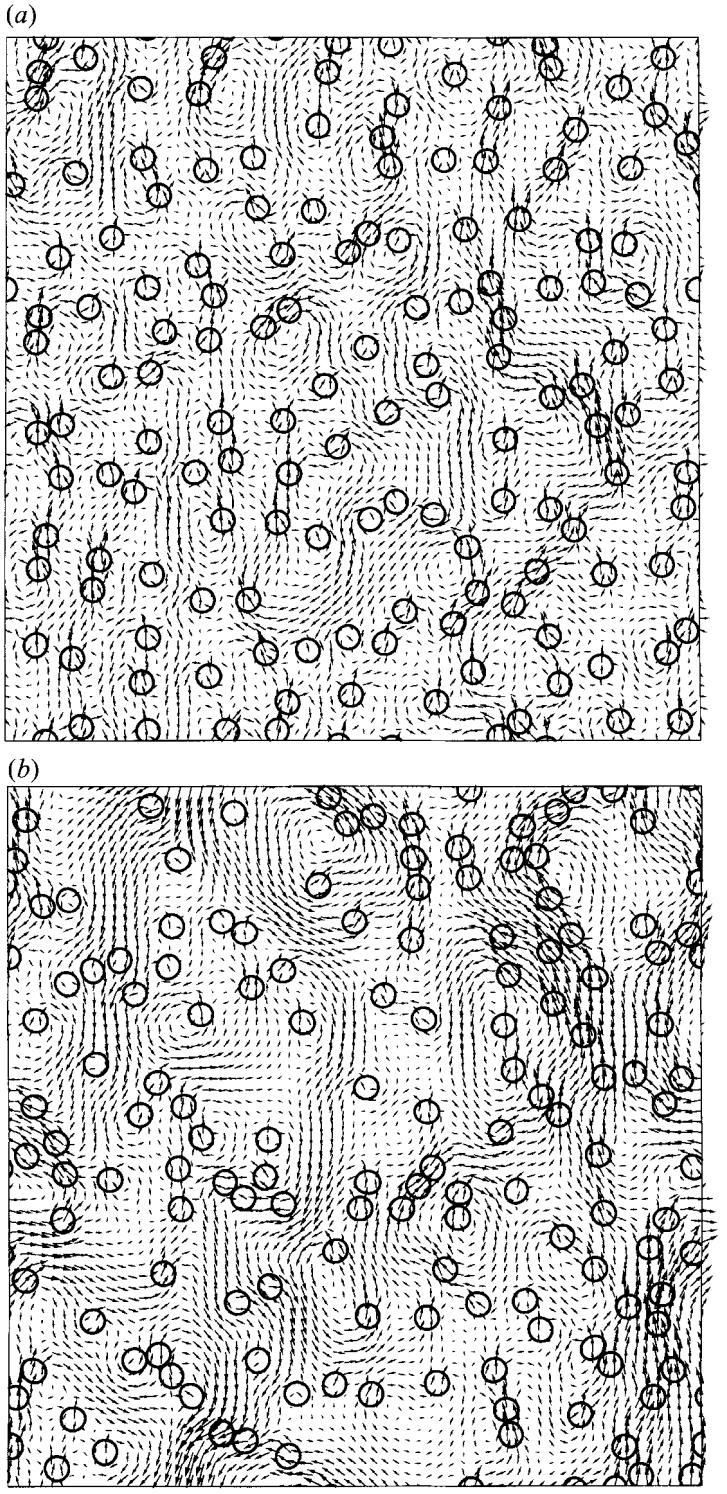

FIGURE 2. Two frames from a simulation of the evolution of 144 bubbles in a doubly periodic box. The bubbles and the velocity field is shown at times 15.8 (*a*) and 175.6 (*b*). The computation is done on a 386^2 grid, but here the velocity vectors are shown at every 6th grid point.

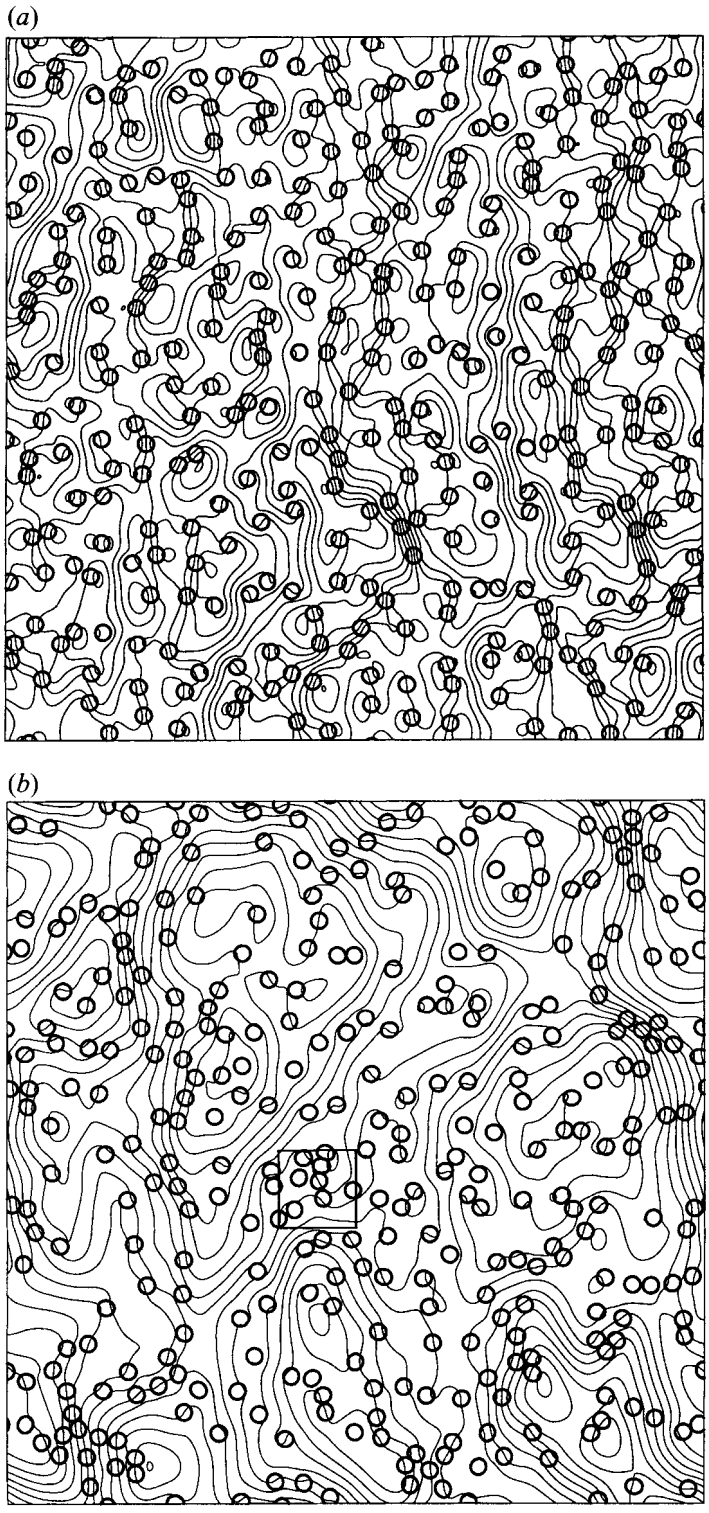

FIGURE 3. Two frames from a simulation of the evolution of 324 bubbles in a doubly periodic box. The bubbles and the streamfunction, with respect to a stationary frame, are shown at times 15.8 (*a*) and 147.9 (*b*). The computation is done on a 578^2 grid.

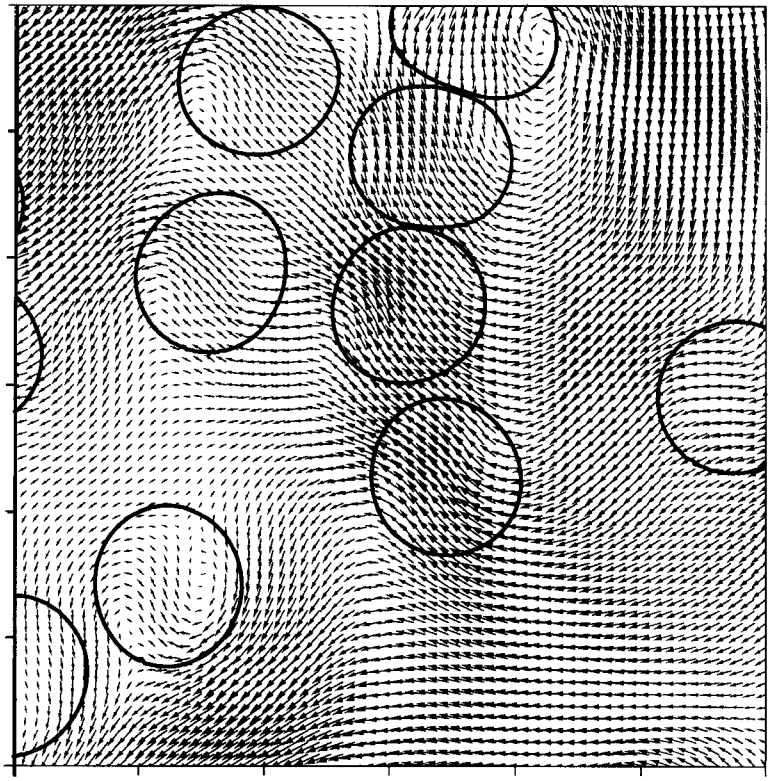

FIGURE 4. An enlarged view of the bubbles and the velocity field in the rectangle drawn in the middle of figure 3(*b*).

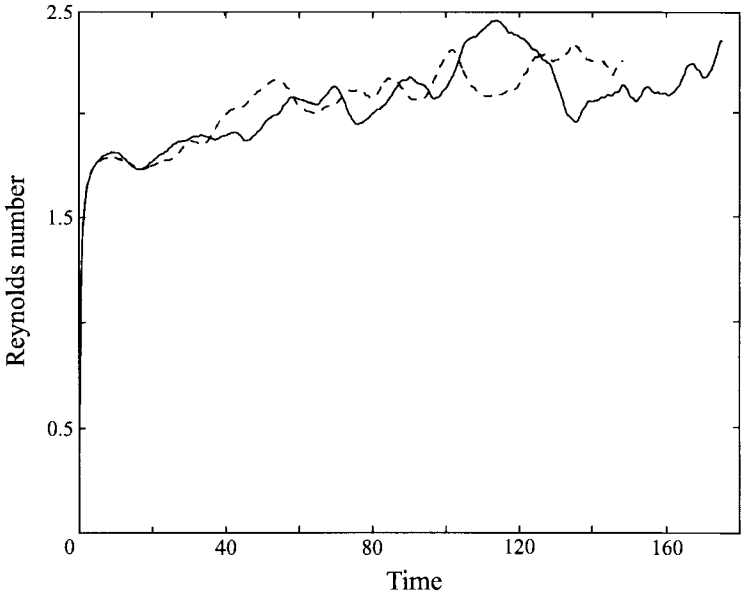

FIGURE 5. The average rise bubble Reynolds number versus time. The results for the 144 bubble simulation are shown by a solid line and the 324 bubble results by a dashed line.

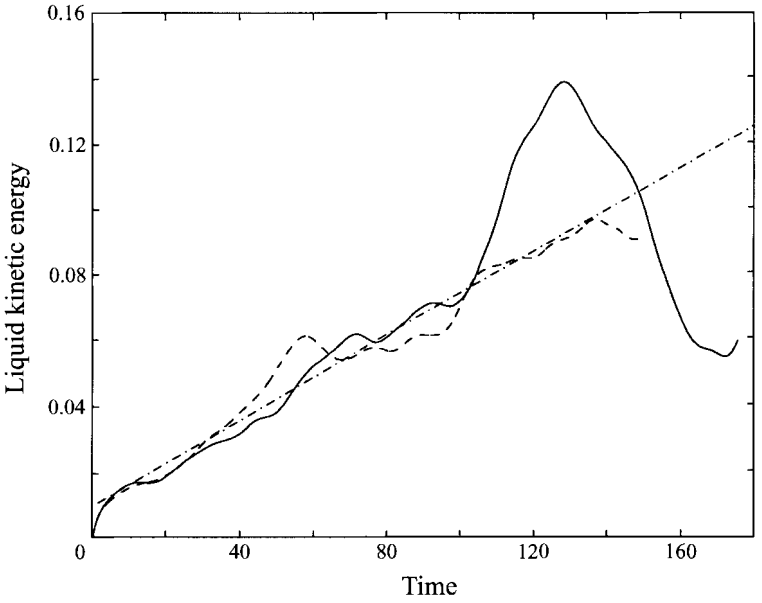

FIGURE 6. The average kinetic energy per unit volume of the ambient liquid, normalized by $\rho_o g d_e$, as a function of time for both the 144 and the 324 bubble simulations. The results for the 144 bubbles are shown by a solid line and the 324 bubble results by a dashed line. The straight line fit is used to estimate the average rate of energy increase.

number is not entirely consistent with the non-dimensionalization used elsewhere in the paper, which would result in $(d_e g)^{1/2}$ as a velocity scale. However, the velocity can be obtained in these units by dividing the Reynolds number by $(N)^{1/2} = 5.6234$. To examine the liquid velocities we plot, in figure 6, the average kinetic energy per unit volume, normalized by $\rho_o g d_e$, versus time for both runs. It is clear that the energy is constantly increasing. This behaviour confirms what we already saw from the velocities and the streamfunction in figures 2 and 3, and is also consistent with the gradual increase in the bubble Reynolds number in figure 5. The reason for the large fluctuations near the end of the computation with fewer bubbles is likely due to length scales that have reached the size of the computational domain. To examine in more detail how the length scales in these flows evolve, we plot in figure 7, the two-dimensional 'kinetic energy' spectrum at three selected times for both the 144 bubble run (*a*) and the 324 bubble run (*b*). The focus here is on the velocity field, and the spectrum is computed from the velocity field in the whole computational domain, irrespective of whether a point is inside or outside a bubble. Therefore, E as defined below is not strictly the kinetic energy, since we have ignored the variation in density between the bubbles and the ambient liquid. When the void fraction is large, there can be a significant difference between E and the true kinetic energy, since the highest velocity is often inside the bubbles. As the void fraction becomes smaller, E approaches the true kinetic energy. To bring out the scaling of the spectrum, $\ln(E)$ is plotted versus $\ln(k)$. The spectrum is computed by first interpolating the velocity onto a 256^2 grid for the 144 bubble run and a 512^2 grid for the 324 bubble case, and then finding the discrete Fourier transform by

$$\tilde{u}_{lj} = \sum_{n=0}^{N-1} \sum_{m=0}^{M-1} u_{nm} e^{(2\pi i n l/N)} e^{(2\pi i m j/M)}. \tag{3.1}$$

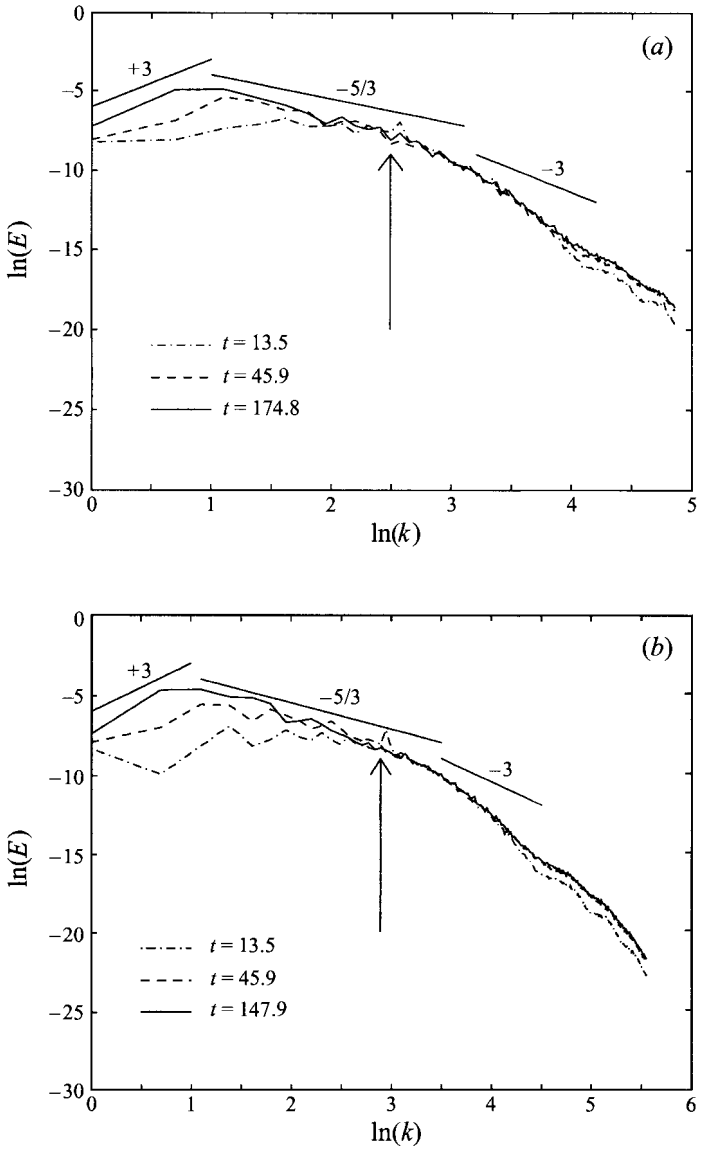

FIGURE 7. The energy spectrum at three times. $\ln(E)$ versus $\ln(k)$. (*a*) The 144 bubble run. (*b*) The 324 bubble run. Lines with slope +3, −5/3, and −3 are included for reference.

N and M are the number of grid points in the horizontal and the vertical directions, respectively (here $N = M$). The energy content of each mode is then computed by

$$E(k) = \sum \tfrac{1}{2}|\tilde{u}_{lj}|^2 \tag{3.2}$$

where $k - 1/2 < (l^2 + j^2)^{1/2} < k + 1/2$. Since the highest wavenumbers are only partially filled, we only plot $k \leqslant 128$ (i.e. $\ln(E) \leqslant 4.85$) for the 144 bubble run and $k \leqslant 256$ (i.e. $\ln(E) \leqslant 5.54$) for the 324 bubble run. Since it is the slope of the energy spectrum that is of most interest, the plot in figure 7 has not been normalized in any way. Non-dimensionalizing the energy and/or the wavenumbers would simply move the curve horizontally or vertically, but not change its shape. The plots in figure 7

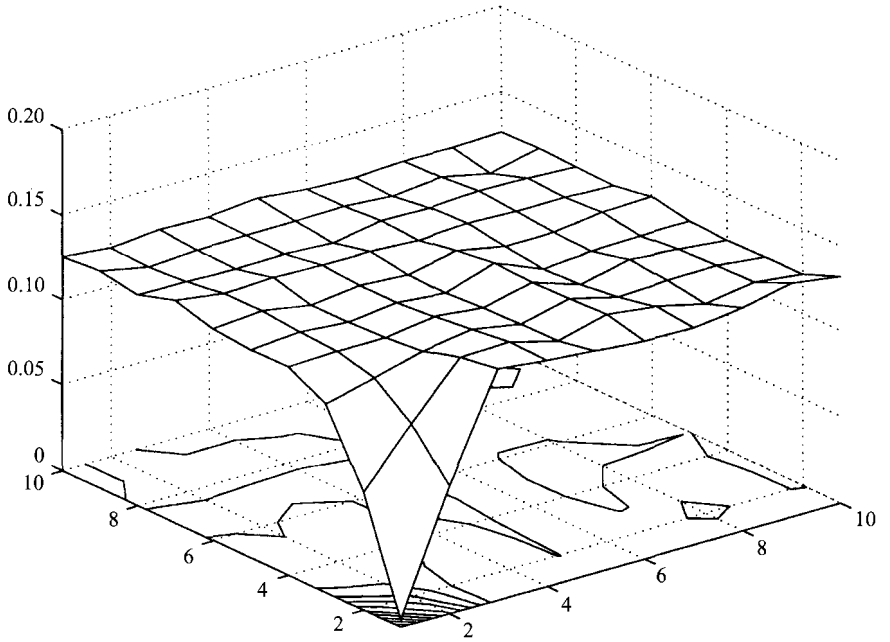

FIGURE 8. The bubble distribution probability density function for the 324 bubble run. The results have been averaged over nine equispaced times. When length is non-dimensionalized by d_e, the average probability distribution function is equal to the void fraction. Twenty equispaced contours are plotted.

show that the small-scale features of the flow have a very well-defined energy spectrum that is nearly identical for both runs and quickly reaches a steady state. At the larger scales both simulations show the same behaviour, but the spectrum is no longer constant with time. Instead we see – although the logarithmic scale used in this plot obscures the differences somewhat – a gradual increase in the energy content of the longest waves. We note that Singh & Joseph (1995) have also presented the energy spectrum of the velocity field. Their analysis, however, was for a one-dimensional model and they were concerned with different questions than those addressed here.

The energy spectrum suggests that the behaviour of the smallest scales in the bubble cloud does not change as the large-scale motion does. To examine the small-scale bubble distribution we have computed the two-dimensional probability distribution function, $P(\Delta x, \Delta y)$, for the bubbles at several times. P shows the probability of finding a bubble at a given position relative to another bubble. To compute it, we first find the relative position of each bubble with respect to all other bubbles and then construct the two-dimensional distribution of relative positions by assigning the value of each relative position to a two-dimensional grid by area weighting. If the grid spacing is Δ, then $\Delta x = \Delta i$, and $\Delta y = \Delta j$, and we can write $P(\Delta x, \Delta y) = P_{ij}$. If N_{ij} is the value of the distribution at each grid point, P_{ij} is given by

$$P_{ij} = \frac{N_{ij}}{N_T \Delta^2}, \tag{3.3}$$

where N_T is the total number of bubble pairs. Each bubble pair is only counted once and we average over the left-hand and the right-hand parts of the plot. To account for the periodicity of the domain, we compute not only the distance from one bubble to another, but also to the corresponding bubbles in adjacent periods, and

use the shortest distance to construct N_{ij}. Since no bubble can be closer to the bubble at the origin than one diameter (if the bubbles remain spherical) the distribution dips down to zero at the origin. For a fine grid, we would expect that $P = 0$ for $r < d$, but since our grid is relatively coarse, P is exactly zero only at the origin. In contrast to the energy spectrum which appears to converge quickly as the number of bubbles is increased, P converges much more slowly and we only show results from the larger run (324 bubbles) in figure 8. P is very 'spiky' at any given time due to the finite number of bubbles involved and the graph in figure 8 is the average over nine evenly spaced times. The mesh size for the grid used to find the probability distribution function in this figure is equal to the bubble diameter, or $\Delta = d_e$, and we plot the results for bubbles within ten diameters of each other. Finer grid results in a more 'spiky' graph. The average probability distribution function over the whole computational domain is simply the void fraction, and the figure shows that on the average the bubbles are nearly uniformly distributed with respect to each other, although near the origin there is a small preference for the bubbles to be side by side, rather than in tandem.

4. Discussion

The most striking feature of the results presented in the previous section is the continuous growth of the low-wavenumber velocity modes. In simulations with a much smaller number of bubbles (Esmaeeli & Tryggvason 1996*a*) we reached a statistically steady state relatively fast. Thus, it appears that the energy of the low-wavenumber velocity modes grows until modes comparable to the size of the computational domain are excited. This suggests that we cannot expect to reach a steady state that is independent of the size of the computational domain. While this behaviour may be a somewhat disappointing result, it should not be unexpected. Indeed, this is exactly what is seen in numerical simulations of two-dimensional turbulence in single-phase fluids, particularly when the motion is forced by random stirring at a given wavenumber. In two-dimensional flows, stretching of vortex tubes, which is the predominant mechanism generating small scales, is absent and mechanisms that generate larger scales, such as the pairing of vortex patches with the same sign vorticity, dominate the dynamics. Both simulations and theoretical arguments (see Lesieur 1991, for example, for a review and discussion) show that the energy spectrum has a $k^{-5/3}$ slope below the forcing frequency where the energy flux is toward larger scales. Thus, while the high-frequency part of the spectrum reaches a steady state, the energy content in the low-wavenumber modes continues to grow until limited by the size of the computational domain. Below the forcing frequency a more rapid decay is observed. The exact slope is a matter of some controversy (see McWilliams 1984) but is generally believed to be at least -3 and most likely more negative. At the very lowest wavenumbers, a k^3 spectrum is found due to non-local interactions between different periods. We have drawn lines with these slopes on the plots of the energy spectrum (figure 7), and although the range of scales is too limited to clearly identify distinct regions, the overall shape of our spectrum is not inconsistent with these slopes. The forcing due to the bubbles is, of course, very different from what is usually used in simulations of two-dimensional homogeneous turbulence. If the bubbles were uniformly distributed, we would have 12 bubbles across the domain for one run and 18 for the other. We have marked the wavenumbers corresponding to forcing at these wavenumbers by an arrow in the plots in figure 7, and although we expect forcing at both higher and lower wavenumbers,

we see a change in the slope near the arrow. At the lowest wavenumbers the spectrum has a positive slope that is close to +3 at the latest time. Then there is a region with an approximately −5/3 slope, and finally there is a more rapid fall-off at wavenumbers above the forcing frequency. The last slope is considerably greater than −3. Since viscous dissipation is already strong at all wavenumbers above the forcing frequency, and the flow is presumably modified by the presence of the bubbles, we do not expect it to be in a very good agreement with the −3 slope or any other slope predicted by theoretical considerations of two-dimensional turbulence. Such theories are based on the assumption that the dynamics is governed by inertial effects, and since the bubble Reynolds number is so low in our case, that assumption is unlikely to be valid here. Although the bubble Reynolds number is relatively low, a Reynolds number based on the domain size is much larger and inertial effects can be significant at larger scales. We note that if the transfer of energy to larger scales is a direct consequence of the nonlinear interactions of flow scales of different sizes (as opposed to resulting from a clustering of the bubbles), the evolution seen here is inherently a finite Reynolds number effect and would not be approximated well by simulations ignoring all inertial effects, such as in, for example, Stokesian Dynamics.

The result suggests that for these low-Reynolds-number flows, the bubbles can be viewed as a stirring force acting on the fluid. The force density, however, is a function of the flow and the bubbles are generally found in the up-flowing region of the large-scale vortices that emerge at later time. This is, of course, in contrast to what we would expect in flows with strong high-Reynolds-number vortices where the bubbles would accumulate in the centre of the vortices. For a steadily rising single bubble, all the work that the bubble does on the liquid is dissipated by viscous action. For a freely evolving array the bubbles arrange themselves in such a way that dissipation is reduced but since (at least initially) the average bubble velocity is nearly the same as for a single bubble, there is 'extra' work available that increases the kinetic energy of the fluid. This increase can be estimated from figure 6. Using a straight line fit to the energy versus time curve, the rate of increase in kinetic energy can be estimated to be 6.8×10^{-4}, in non-dimensional units. The rate of work per unit volume done on the fluid by the bubbles, if we neglect completely the density of the bubbles, is (in dimensional units)

$$\dot{w} = \rho_o g \alpha (1 - \alpha) U_B \tag{4.1}$$

where U_B is the average rise velocity of the bubbles. If we non-dimensionalize the work in the same way as the energy, scale velocity by $(gd_e)^{1/2}$, and use the rise velocity of a single bubble (0.2767 in these units), we find that $\tilde{\dot{w}} = \alpha(1 - \alpha)\tilde{U}_B = 3.04 \times 10^{-2}$ (denoting the non-dimensional variables by a tilde). Therefore, slightly more than 2% of the work is fed to the larger scales. We suspect that this fraction depends strongly on the bubble Reynolds number.

The average evolution of the bubbles is likely to depend sensitively on how the bubbles are distributed, on the average. For Stokes flows, theoretical estimates of the sedimentation rate of rigid spheres result, in some cases, in a linear relation between sedimentation rate and void fraction for dilute systems (Batchelor 1972), whereas in other cases it is found that sedimentation rate depends on the cubic root of the void fraction (Happel & Brenner 1965). Davis & Acrivos (1985) show that these two forms correspond to two limiting cases for the probability density function, namely a completely random distribution where the probability of finding a bubble at a given relative position to another bubble is constant, and a uniform distribution where the nearest neighbour separation is approximately equal to the

average separation. Our results clearly indicate that the former is the case for our system, although the probability density function suggests that the bubbles spend a slightly longer time in a side by side configuration than in a tandem one. We also note that we observe transient structures, mostly as a result of the 'drafting, kissing, and tumbling' mechanism of Fortes, Joseph, & Lundgren (1987), but we have not seen the formation of horizontal layers like those observed by Fortes *et al.* for particles in a narrow channel and predicted by inviscid simulations (except for the slight asymmetry in P). This is not surprising since the forces responsible for the layer formation are primarily inviscid, and Singh & Joseph (1995) found that the layers are not as observable at $Re = 300$ as they are for Reynolds numbers over a thousand. Here, the bubble Reynolds number is less than 2.

While there is a net upward flow of bubbles that is larger than one would expect from results for a regular array (Esmaeeli & Tryggvason 1996*a*), one might ask why the bubbles do not all accumulate into an upward moving stream. Clearly, there is a tendency for the bubbles to come together and form such streams! We do not yet understand why the streams seem to break up as soon as they form and why so many bubbles are contained in regions of down flow, but offer the following two speculations. First, it is known that two bubbles in tandem is an unstable configuration and while bubbles are drawn into the wake of each other, they 'tumble' after collision and the bubble behind catches up with the one in front (the 'drafting, kissing, and tumbling' mechanism of Joseph and collaborators). At low Reynolds numbers, close bubbles in a side by side configuration repel each other (exactly opposite to what happens at higher Reynolds numbers, see Kim, Elghobashi, & Sirignano 1993, and Jan 1993) and it is possible that some bubbles are 'pushed out' of the stream by other bubbles. The other explanation relies on the lift force on the bubbles. Spherical (and cylindrical) bubbles moving upward in a vertical shear are driven toward the downward moving fluid and would thus be driven out of the upward moving stream. Since the direction of the lift force is very sensitive to the deformations of the bubbles (Kariyasaki 1987; Ervin & Tryggvason 1996; Esmaeeli, Ervin, & Tryggvason 1993), a cloud with more deformable bubbles might behave differently.

5. Conclusion

We have presented numerical results that suggest strongly that a two-dimensional low-Reynolds-number bubbly flow will continuously evolve toward a state containing larger and larger scales. This evolution will continue until the largest scales become comparable to the size of the computational domain. Thus, we cannot expect to reach a statistically steady state that is independent of the size of the system. While these are somewhat disappointing results from a modelling standpoint, where we would like to be able to obtain fully converged statistics using modest size systems, the same result is well known from simulations of forced two-dimensional turbulence in homogeneous flows, where the flow scales continue to grow until they reach the size of the computational domain. The similarity between these two flows suggests that the fluid 'feels' the effect of the bubbles mainly as a high-wavenumber forcing which pumps energy into the flow and excites the larger scales through nonlinear interactions. While the increase in the energy content of the larger scales is a two-dimensional phenomenon, it is possible that this model – that the bubbles can be treated as a small-scale 'stirring force' – is applicable to fully three-dimensional flows.

Although we believe that the continuous growth of the scales here is a finite-Reynolds-number phenomenon, we note that continuous growth of the average length

scale is seen in flows at zero Reynolds number. The emergence of a single large finger in the Taylor–Saffman instability in a Hele-Shaw cell for a large viscosity contrast (see, for example, Tryggvason & Aref 1985) and the formation of large-scale 'channels' in suspensions of polydispersed particles in Stokes flow (Davis & Acrivos 1985) are two examples. Indeed, Revay (1992) concluded, based on his simulations using continuum models for bidispersed sedimentation in periodic domains, that his systems evolved continuously toward larger scales and that the final state depended on the size of the computational domain.

From a practical point of view, two questions remain unanswered. First, what happens in three dimensions? If the analogy with two-dimensional turbulence holds, then we would expect three-dimensional motion to continually regenerate smaller scales. Injection of bubbles into large containers is known to lead to large recirculation regions, but in those situations the bubbles are generally injected in a very confined area, thus imposing a forcing very different from what we have here. Second, what happens at higher Reynolds numbers? In Esmaeeli & Tryggvason (1996*b*) we have already shown that clouds of bubbles at higher Reynolds numbers behave fundamentally differently from low Reynolds number clouds. While the rise velocity of a freely evolving low-Reynolds-number cloud is higher than that of a uniform distribution of bubbles, the opposite is true at higher Reynolds numbers. Thus, it seems possible that higher-Reynolds-number flows would exhibit different behaviour, even in two dimensions. The mechanisms that we suggested to explain the breakup of the streams of bubbles that appeared in the freely evolving array are also different at higher Reynolds numbers. Moreover, it is possible that the deformability of the bubbles could significantly influence the mechanisms discussed above. We hope to return to these questions in the future.

This work was supported by the National Science Foundation grant CST-913214. We would like to acknowledge constructive discussions with Professor R. Akhavan, and the help of Mr R. Gundlapalli in computing the energy spectrum. We also thank Professor J. Higdon for sending us a copy of the Thesis by Revay. Preliminary computations were done on the computers at the San Diego Supercomputer Center which is sponsored by the NSF, but the results reported here were computed at the Center for Parallel Computing (CPC) at the University of Michigan. We would like to thank Dr H. Marshall for his help with using the CPC facilities and Dr John Adams at NCAR for sending us a copy of his latest version of MUDPACK.

REFERENCES

ADAMS, J. 1989 MUDPACK: Multigrid Fortran Software for the Efficient Solution of Linear Elliptic Partial Differential Equations. *Appl. Maths Comput.* **34**, 113.

BATCHELOR, G. K. 1972 Sedimentation in a dilute dispersion of spheres. *J. Fluid Mech.* **52**, 245–268.

BRADY, J. F. 1993 Stokesian dynamics simulation of particulate flows. In *Particulate Two-Phase Flow* (ed. M. C. Roco), pp. 912–950. Butterworth.

BRADY, J. F. & BOSSIS, G. 1988 Stokesian Dynamics. *Ann. Rev. Fluid Mech.* **20**, 111–157

CLIFT, R., GRACE, J. R. & WEBER, M. E. 1978. *Bubbles, Drops, and Particles.* Academic.

DAVIS, R. H. & ACRIVOS, A. 1985 Sedimentation of noncolloidal particles at low Reynolds numbers. *Ann. Rev. Fluid Mech.* **17**, 91–118.

DREW, D. A. 1983 Mathematical modelling of two-phase flow. *Ann. Rev. Fluid Mech.* **15**, 261–291.

DREW, D. A. & LAHEY, R. T. JR. 1993 Analytical modelling of multiphase flow. In *Particulate Two-Phase Flow* (ed. M. C. Roco), pp. 509–566. Butterworth.

ERVIN, E. A. & TRYGGVASON, G. 1996 The rise of bubbles in a vertical shear flow. Submitted to *J. Fluid Engng.*

ESMAEELI, A. 1995 Numerical simulations of bubbly flows. PhD Thesis, The University of Michigan, Ann Arbor.

ESMAEELI, A., ERVIN, E. A. & TRYGGVASON, G. 1993 Numerical simulations of rising bubbles. In *Bubble Dynamics and Interfacial Phenomena. Proc. IUTAM Symp. Birmingham, U.K., 6-9 September 1993* (ed. J. R. Blake, J. M. Boulton-Stone & N. H. Thomas), pp. 247–255. Kluwer.

ESMAEELI, A. & TRYGGVASON, G. 1996*a* Direct numerical simulations of bubbly flows I-Low Reynolds number arrays. Submitted to *J. Fluid Mech.*

ESMAEELI, A. & TRYGGVASON, G. 1996*b* Direct numerical simulations of bubbly flows II-Moderate Reynolds number arrays. In preparation.

FENG, J., HU, H. H. & JOSEPH, D. D. 1994 Direct simulation of initial value problems for the motion of solid bodies in a Newtonian fluid. Part 1. Sedimentation. *J. Fluid Mech.* **261**, 95–134

FORTES, A., JOSEPH, D. D. & LUNDGREN, T. 1987 Nonlinear mechanics of fluidization of beds of spherical particles. *J. Fluid Mech.* **177**, 467–483.

HAPPEL, J. & BRENNER, H. 1965 *Low Reynolds Number Hydrodynamics.* Prentice-Hall.

JAN, Y.-J. 1993 Computational studies of bubble dynamics. PhD Thesis, The University of Michigan, Ann Arbor.

JAN, Y.-J. & TRYGGVASON, G. 1996 A computational study of contaminated bubbles at finite Reynolds numbers. Submitted to *Phys. Fluids.*

KARIYASAKI, A. 1987 Behaviour of a single gas bubble in a liquid flow with a linear velocity profile. In *Proc. 1987 ASME-JSME Thermal Engineering Joint Conf.*, pp. 261–267.

KIM, I., ELGHOBASHI, S. E. & SIRIGNANO, W. A. 1993 Three-dimensional flow over two spheres placed side by side. *J. Fluid Mech.* **246**, 465–488.

LESIEUR, M. 1991 *Turbulence in Fluids. Stochastic and Numerical Modelling.* Kluwer.

MANGA, M. & STONE, H. A. 1993 Buoyancy-driven interactions between deformable drops at low Reynolds numbers. *J. Fluid Mech.* **256**, 647–683.

MCWILLIAMS, J. C. 1984 The emergence of isolated coherent vortices in turbulent flow. *J. Fluid Mech.* **146**, 21–43.

REVAY, J. M. 1992 Mechanics of polydispersed suspensions. PhD Thesis, University of Illinois at Urbana-Champaign.

RYSKIN, G. & LEAL L. G. 1984 Numerical solution of free-boundary problems in fluid mechanics. Part 2. Buoyancy-driven motion of a gas bubble through a quiescent liquid. *J. Fluid Mech.* **148**, 19–35.

SANGANI, A. S. & DIDWANIA, A. K. 1993 Dynamic simulations of flows of bubbly liquids at large Reynolds numbers. *J. Fluid Mech.* **250**, 307–337.

SANGANI, A. S. & PROSPERETTI, A. 1993 Numerical simulation of the motion of particles at large Reynolds numbers. In *Particulate Two-Phase Flow* (ed. M. C. Roco), pp. 971–998. Butterworth.

SINGH, P. & JOSEPH, D. D. 1995 Dynamics of fluidized suspensions of spheres of finite size. *Intl J. Multiphase Flow* **21**, 1–26.

SMEREKA, P. 1993 On the motion of bubbles in a periodic box. *J. Fluid Mech.* **254**, 79–112.

TRYGGVASON, G. & AREF, H. 1985 Finger interaction mechanisms in stratified Hele-Shaw flow. *J. Fluid Mech.* **154**, 284–301.

UNVERDI, S. O. & TRYGGVASON, G. 1992*a* A front-tracking method for viscous, incompressible, multi-fluid flows. *J. Comput. Phys.* **100**, 25–37.

UNVERDI, S. O. & TRYGGVASON, G. 1992*b* Computations of multi-fluid flows. *Physica* D **60**, 70–83.

ZHOU, H. & POZRIKIDIS, C. 1993 The flow of ordered and random suspensions of two-dimensional drops in a channel. *J. Fluid Mech.* **255**, 103–127.

ZHOU, H. & POZRIKIDIS, C. 1994 Pressure-driven flow of suspensions of liquid drops. *Phys. Fluids* **6**, 80–94.